



# Fractional Order Complementary Non-singular Terminal Sliding Mode Control of PMSM Based on Neural Network

Jinliang Zhang<sup>1</sup> · Dunbin Zhu<sup>1</sup> · Wei Jian<sup>1</sup> · Wentao Hu<sup>1</sup> · Guosheng Peng<sup>1</sup> · Yufeng Chen<sup>1</sup> · Zhihu Wang<sup>2</sup>

Received: 8 June 2023 / Revised: 19 September 2023 / Accepted: 26 September 2023 / Published online: 19 February 2024

© The Author(s), under exclusive licence to The Korean Society of Automotive Engineers and Springer-Verlag GmbH Germany, part of Springer Nature 2024

## Abstract

Aiming at the sensitivity problems of uncertain factors such as parameter variation, external disturbance and friction for the permanent magnet synchronous motor control system of electric vehicle, a fractional order complementary non-singular terminal sliding mode control method based on neural network is proposed. The mathematical model of permanent magnet synchronous motor with uncertain factors was established. The sliding mode controller was designed by combining the generalized sliding mode surface and the complementary sliding mode surface, which shortened the arrival time from the state trajectory to sliding mode surface. The fractional calculus operator with filtering characteristics was used to improve the position tracking accuracy and reduce the chattering. As for the variety of uncertain disturbances, the neural network was used to estimate the system total uncertainty and compensate online to further improve the dynamic response ability and anti-interference ability. Finally, the simulation results verify the effectiveness and feasibility of the proposed method, which can provide theoretical and technical support for improving the control accuracy of permanent magnet synchronous motor and the development of electric vehicles.

**Keywords** Permanent magnet synchronous motor · Fractional order complementary · Neural network · Electric vehicle drive system · Non-singular terminal sliding mode

## 1 Introduction

Permanent magnet synchronous motor (PMSM) is widely used in the field of electric vehicle drive system because of its simple structure, high power density, high reliability and small space occupation. However, PMSM is a nonlinear, multivariable and strongly coupled system, which makes it difficult to improve its dynamic and static performance due to the external disturbances, parameter disturbances and other effects (Cai et al., 2017). In recent years, some relevant scholars have proposed a variety of control strategies to suppress the uncertain interference of the system and improve the related performance of the control system; such as sliding mode control (Li et al., 2023), active disturbance

rejection control (Cao et al., 2023; Xu et al., 2023; Xu et al., 2023), neural network control (Li et al., 2022; Lu et al., 2015; Yu et al., 2015), model predictive (Bai et al., 2022; Zhang et al., 2021), etc.

Sliding mode control (SMC) is widely used because of its strong robustness and insensitivity to external reactions (Wang, 2020). However, there are problems of control discontinuity and chattering, so in most cases, other control methods need to be combined to achieve better control effect. In Li et al., (2021), a back-stepping non-singular terminal sliding mode control method with finite time disturbance observer is proposed, where the load torque disturbance is assumed to change slowly and the load is bounded. In Du et al., (2022), the super-twisting sliding mode algorithm is introduced into the active disturbance rejection control by combining active disturbance rejection control and sliding mode control, and the nonlinear state error feedback control rate and tracking differentiator are optimized to improve the fast performance of the system. Li et al., (2021) designed a fractional order sliding mode surface for permanent magnet synchronous motor speed control system, through the fractional order calculus operator unique memory characteristics

✉ Jinliang Zhang  
zhangjl\_dy@huat.edu.cn

<sup>1</sup> School of Electrical and Information Engineering, Hubei University of Automotive Technology, Shiyan 442002, People's Republic of China

<sup>2</sup> Dongfeng Automobile Power Parts Co. Ltd, Shiyan 442002, People's Republic of China

and genetic characteristics to suppress the chattering problem, but the dynamic response ability of the system is poor. Jin, (2021) introduced fuzzy control on the basis of fractional sliding mode, and used fuzzy algorithm to realize online adaptive adjustment of sliding mode switching term and fractional order, but the article did not consider the suppression and compensation of external disturbances. Jin and Zhao, (2019) added a complementary sliding mode surface based on the generalized sliding mode surface, and introduced Elman neural network to estimate the uncertainty interference, which can improve the position tracking accuracy of the system. In Jin and Zhao, (2020), the complementary sliding mode control and iterative learning in intelligent control are combined. This method can effectively suppress the influence of uncertainty on the system, thus accelerating the convergence speed of the controller and improving the convergence accuracy.

To further improve the anti-interference ability of the system, a control method combining neural network and fractional order complementary non-singular terminal sliding mode controller is designed in this paper. First, a non-singular terminal sliding mode is introduced to design the controller by combining the generalized sliding mode surface and complementary sliding mode surface, which can converge in finite time to solve the system singularity problem. It can shorten the time for the state trajectory to reach the sliding mode surface and also reduce the system chattering. On this basis, the fractional order calculus operator with filtering characteristics was adopted to improve the position tracking accuracy and reduce the steady-state error. Besides, the neural network is used to approximate the disturbance and un-modeled parts of the system to further improve the dynamic response ability and anti-interference ability of the system. The experimental results show that the proposed control method has the advantages of fast response speed, high tracking accuracy and small steady-state error, and it can effectively suppresses external uncertain interference.

This paper is organized as follows. The mathematical model of PMSM is reviewed in Sect. 2. The whole system control strategies are presented in Sect. 3, and fractional order complementary sliding mode and RBF neural network are designed in detail in this section. The simulation experiments are carried out and the results are analyzed with the conditions of speed step, load step and parameter change in Sect. 4. Finally, some conclusions are given in Sect. 5

## 2 Mathematical Model of PMSM

According to the principle of field oriented control, the dynamic model of PMSM in synchronous rotating coordinate system is established as follows:

$$\begin{cases} u_d = Ri_d - \omega L_q i_q + L_d \frac{d}{dt} i_d \\ u_q = Ri_q + \omega L_d i_d + \omega \psi_f + L_q \frac{d}{dt} i_q \end{cases}, \quad (1)$$

where  $u_d$  and  $u_q$  are stator voltages;  $i_d$  and  $i_q$  are stator current;  $L_d$  and  $L_q$  are stator inductance;  $R$  is stator resistance;  $\omega$  is mechanical angular velocity; and  $\psi_f$  is permanent magnet flux linkage.

As for surface-mounted PMSM,  $L_d = L_q$ . Therefore, the electromagnetic torque in the synchronous rotating coordinate system is

$$T_e = \frac{3}{2} p_n \psi_f i_q, \quad (2)$$

where  $P_n$  is the number of pole-pairs.

The motor motion equation can be described as

$$\frac{d\omega}{dt} = \frac{T_e}{J} - \frac{T_L}{J} - \frac{B}{J} \omega, \quad (3)$$

where  $T_L$  is load torque;  $T_e$  is electromagnetic torque;  $B$  is the damping coefficient and  $J$  is the moment of inertia.

Substitute (2) into (3), it can be obtained as:

$$\begin{cases} \dot{\omega} = a\omega + bi_q + c \\ a = -\frac{B}{J}, b = \frac{3p_n\psi_f}{2J}, c = -\frac{T_L}{J} \end{cases}. \quad (4)$$

Considering the variation of motor parameters and un-modeled uncertainty in the different working condition and external environment, Eq. (4) can be expressed as

$$\dot{\omega} = (a + \Delta a)\omega + (b + \Delta b)i_q + (c + \Delta c), \quad (5)$$

where  $\Delta a, \Delta b, \Delta c$  are uncertain disturbances of motor parameters.

The speed tracking error is defined as  $e = \omega^* - \omega$ ,  $\omega^*$  as the reference speed. Its derivation can be obtained by

$$\begin{cases} \dot{e} = ae - bi_q - a\omega^* - F \\ F = \Delta a\omega + \Delta b i_q + \Delta c + c \end{cases}, \quad (6)$$

where  $F$  is the total uncertainty disturbances.

## 3 Design of Fractional Order Complementary Sliding Mode Controller

### 3.1 Fractional Calculus Theory

Fractional calculus is a generalized on the basis of integer order calculus. It can describe the dynamic characteristics of motor model more accurately. Fractional calculus operator is usually expressed by  ${}_h D_t^\alpha$ , which is defined as

$${}_h D_t^\alpha = \begin{cases} \frac{d^\alpha}{dt^\alpha} & R(\alpha) > 0 \\ 1 & R(\alpha) = 0 \\ \int_h^t (d\tau)^{(-\alpha)} & R(\alpha) < 0 \end{cases} \quad (7)$$

where  $t$  and  $h$  are the upper and lower bounds of the integral operator;  $\alpha$  is the order of the differential operator;  $R(\alpha)$  is the real part of  $\alpha$ , and the upper and lower bounds are not considered in the following, so the fractional order is represented by  $D^\alpha$ .

There are many definitions of fractional calculus, such as Grunwald–Letnikov, Riemann–Liouville, and Caputo. The third one (Caputo) is adopted in this paper (Podlubny, 1999)

$${}_h D_t^\alpha f(t) = \frac{1}{\Gamma(m - \alpha)} \int_h^t \frac{f^{(m)}(\tau)}{(t - \tau)^{\alpha - m + 1}} d\tau, \quad (8)$$

where  $\Gamma(x)$  is the gamma function.  $0 \leq m - 1 < \alpha < m$ .

Lemma 1: Let  $x(t) \in R_n$  be a vector of a differentiable function. When  $t \geq t_0$ , the following relation is established (Duarte-Mermoud et al., 2015):

$$\begin{cases} \frac{1}{2} D^\alpha [x^T(t) P x(t)] \leq x^T(t) P D^\alpha x(t) \\ \forall \alpha \in (0, 1] \end{cases} \quad (9)$$

Since the value of fractional calculus cannot obtain an accurate numerical solution, an improved Oustaloup filter is used to approximate. And the filter formula with the filtering frequency band of  $(\omega_b, \omega_h)$  is

$$s^\alpha \approx K \left( \frac{d\omega_h}{l} \right)^\alpha \left( \frac{ds^2 + l\omega_h s}{d(1-\alpha)s^2 + l\omega_h s + d\alpha} \right) \prod_{k=-N}^N \frac{s + \omega_k^*}{s + \omega_k} \quad (10)$$

The zero pole and gain of filter are

$$\begin{cases} \omega_k^* = \omega_b \omega_u^{(2k-1-\alpha)/N} \\ \omega_k = \omega_b \omega_u^{(2k-1+\alpha)/N} \\ K = \omega_h^\alpha \\ \omega_u = \sqrt{\omega_h / \omega_b} \end{cases}, \quad (11)$$

where  $l$  and  $d$  are weight parameters.

Through the filter, it can output more accurate approximation of fractional calculus.

### 3.2 Design of Fractional Order Complementary Sliding Mode Controller

Complementary sliding mode control (CSMC) adds a complementary sliding mode surface to the traditional SMC. The added complementary sliding mode surface can make the system have higher tracking accuracy and response speed, and also improve the system robustness. Fractional order sliding

mode control (FOSMC) introduces fractional order calculus on the basis of SMC. Fractional order differential operator has the advantages of slow energy transfer, memory and heredity, and it can describe the dynamic characteristics of motor model more accurately. Fractional order complementary sliding mode control (FOCSMC) combines CSMC and FOSMC to decrease the chattering and increase the degree of operation freedom; it further improves the speed tracking ability of PMSM control system.

The sliding mode surface is composed of generalized sliding mode surface  $S_g$  and complementary sliding mode surface  $S_c$ , and the sliding mode control law is composed of equivalent control law  $i_{eq}$  and switching control law  $i_v$ .

The generalized non-singular terminal sliding surface is designed as

$$S_g = D^\alpha e + 2\lambda e + \lambda^2 D^{-\alpha} (e + c_1 |e|^\beta \text{sgn}(e)). \quad (12)$$

The complementary non-singular terminal sliding surface is designed as

$$S_c = D^\alpha e - \lambda^2 D^{-\alpha} (e + c_1 |e|^\beta \text{sgn}(e)), \quad (13)$$

where  $\lambda$  is a positive number.  $0 < \alpha < 1, 0 < \beta < 1, c_1 > 0$ .

Derivation of Eqs. (12) and (13) is driven as

$$\begin{aligned} D^\alpha S_g &= D^{2\alpha} e + 2\lambda D^\alpha e + \lambda^2 (e + c_1 |e|^\beta \text{sgn}(e)) \\ D^\alpha S_c &= D^{2\alpha} e - \lambda^2 (e + c_1 |e|^\beta \text{sgn}(e)). \end{aligned} \quad (14)$$

Combining the formulas (12) and (13), the sum of the sliding surfaces is obtained

$$S_{\text{sum}} = S_g + S_c = 2(D^\alpha e + \lambda e). \quad (15)$$

And there are the following relationships:

$$\begin{aligned} \lambda S_{\text{sum}} &= 2\lambda(D^\alpha e + \lambda e) \\ &= D^\alpha S_g - D^\alpha S_c - 2c_1 \lambda^2 |e|^\beta \text{sgn}(e). \end{aligned} \quad (16)$$

Let the Lyapunov function as  $V_1 = (S_g^2 + S_c^2)/2$ , combining lemma 1, the  $\alpha^{\text{th}}$  derivative of  $V_1$  is obtained (Liu, 2021)

$$\begin{aligned} D^\alpha V_1 &= \frac{1}{2} D^\alpha S_g^2 + \frac{1}{2} D^\alpha S_c^2 \leq S_g D^\alpha S_g \\ &\quad + S_c D^\alpha S_c = S_g D^\alpha S_g \\ &\quad + S_c (D^\alpha S_g - \lambda S_{\text{sum}} - 2c_1 \lambda^2 |e|^\beta \text{sgn}(e)) \\ &= S_{\text{sum}} (D^\alpha S_g - \lambda S_c) - 2c_1 \lambda^2 S_c |e|^\beta \text{sgn}(e) \\ &= S_{\text{sum}} [D^{2\alpha} e + \lambda^2 (e + c_1 |e|^\beta \text{sgn}(e)) \\ &\quad - \lambda S_c + 2\lambda D^\alpha e] - 2c_1 \lambda^2 S_c |e|^\beta \text{sgn}(e) \\ &= S_{\text{sum}} [D^{2\alpha-1} (ae - bi_q - a\omega^* - F) \\ &\quad + 2\lambda D^\alpha e + \lambda^2 (e + c_1 |e|^\beta \text{sgn}(e)) - \lambda S_c] \\ &\quad - 2c_1 \lambda^2 S_c |e|^\beta \text{sgn}(e). \end{aligned} \quad (17)$$

The fractional order complementary sliding mode control law is composed of equivalent control law and switching control law. It can be expressed as  $i_q^* = i_{eq} + i_v$ .

To ensure stability, the equivalent control law can be designed as

$$i_{eq} = \frac{1}{b} \left[ -a\omega - F + 2\lambda D^{1-\alpha} e + \lambda D^{1-2\alpha} S_g + \lambda^2 D^{1-2\alpha} (e + (c_1 - 2c_1 \frac{S_c}{S_{sum}}) |e|^\beta \text{sgn}(e)) \right]. \tag{18}$$

The switching control law is selected as

$$i_v = \frac{\rho}{b} \left[ D^{1-2\alpha} \text{sat} \left( \frac{S_{sum}}{\theta} \right) \right], \tag{19}$$

where  $\text{sat}(\cdot)$  is the saturation function,  $\theta > 0$  is the boundary layer thickness, and  $\rho > 0$  is the control gain

$$\text{sat} \left( \frac{S_{sum}}{\theta} \right) = \begin{cases} 1 & S_{sum} \geq \theta \\ \frac{S_{sum}}{\theta} & -\theta < S_{sum} < \theta \\ -1 & S_{sum} \leq -\theta \end{cases}. \tag{20}$$

Substituting the above equation into Eq. (17)

$$D^\alpha V_1 \leq -\lambda S_{sum}^2 - \rho S_{sum} \text{sat} \left( \frac{S_{sum}}{\theta} \right) \leq 0. \tag{21}$$

It can be seen from formula (21) that the controller satisfies the Lyapunov stability theorem. Therefore, the control law is designed as

$$i_q^* = \frac{1}{b} \left[ -a\omega - \hat{F} + 2\lambda D^{1-\alpha} e + \lambda D^{1-2\alpha} S_g + \lambda^2 D^{1-2\alpha} (e + (c_1 - 2c_1 \frac{S_c}{S_{sum}}) |e|^\beta \text{sgn}(e)) + \rho D^{1-2\alpha} \text{sat} \left( \frac{S_{sum}}{\theta} \right) \right]. \tag{22}$$

### 3.3 Design of Fractional Order Complementary Sliding Mode Controller Based on RBF Neural Network

There are uncertain factors such as parameter changes and external disturbances during the system operation, which have adverse effects on the control performance. As for the uncertain disturbances in Eq. (22), RBF neural network is used to approximate the disturbance and un-modeled parts online and compensate them to further improve the system control performance (Liu, 2014a, 2014b). The structure of RBF neural network is shown in Fig. 1.

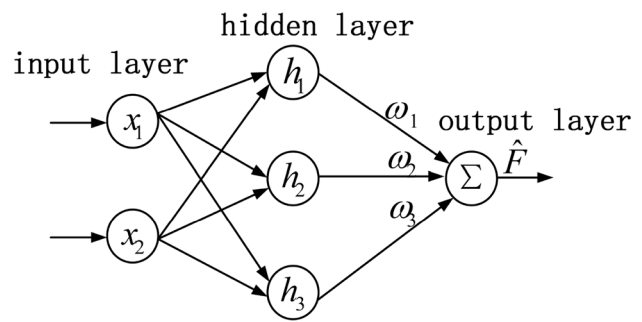


Fig. 1 Neural network structure model

The speed error and speed error change rate are used as the input of RBF neural network. Based on the above structure,  $x = [x_1 \ x_2]^T = [e \ \dot{e}]^T$ . The hidden layer function of RBF neural network is selected as

$$h_j(x) = \exp \left( -\frac{\|x - c_j\|^2}{2b_j^2} \right), \tag{23}$$

where  $c_j$  is the center vector of the  $j$ th node function;  $b_j$  is the base width parameter of the  $j$ th hidden layer node function.

The output of RBF neural network is the sum of the weighted product of each hidden layer neuron output value and corresponding connection weight, which is represented as

$$y = \sum_{j=1}^n \omega_j h_j(x). \tag{24}$$

The formula above is rewritten in vector form as

$$\hat{F} = W^T \varphi, \tag{25}$$

where  $W = [\omega_1 \ \dots \ \omega_n]^T$  is the RBF neural network connection weight vector;  $\varphi = [h_1 \ \dots \ h_n]^T$  is the RBF neural network hidden layer output vector.

RBF neural network can approximate any nonlinear function. Selecting appropriate  $c_j, b_j$  and  $\omega_j$  can improve the accuracy of approximation. The selection of  $c_j$  is determined according to the input value range of the network. The parameter  $b_j$  determines the mapping ability of the network input, which is generally designed as a moderate value. And the parameter  $\omega_j$  is designed by Lyapunov stability analysis.

Define  $\tilde{w} = w - \hat{w}$  as the error between the ideal optimal value and the estimated value of the weight, and select the Lyapunov function

$$V_2 = \frac{1}{2} (S_g^2 + S_c^2) + \frac{1}{2} \gamma D^{2\alpha-1} \tilde{W}^T \tilde{W}, \tag{26}$$

where  $\gamma$  is the adaptive coefficient of neural network weight.

By taking the  $\alpha$ th derivative of Eq. (26) and combining with Lemma 1, Eq. (16), Eq. (22) and Eq. (25), it can be obtained

$$\begin{aligned}
 D^\alpha V_2 &\leq S_g D^\alpha S_g + S_c D^\alpha S_c + \gamma D^{2\alpha-1} \tilde{W}^T D^\alpha \tilde{W} \\
 &\leq S_{\text{sum}} \left[ D^{2\alpha-1} (ae - bi_q - a\omega^* - F) + 2\lambda D^\alpha e \right. \\
 &\quad \left. + \lambda^2 (e + c_1 |e|^\beta \text{sgn}(e)) - \lambda S_c \right] \\
 &\quad - 2c_1 \lambda^2 S_c |e|^\beta \text{sgn}(e) + \gamma D^{2\alpha-1} \tilde{W}^T D^\alpha \tilde{W} \\
 &= S_{\text{sum}} \left[ D^{2\alpha-1} (F - \hat{F}) - \rho \text{sat} \left( \frac{S_{\text{sum}}}{\theta} \right) \right] \\
 &\quad + \gamma D^{2\alpha-1} \tilde{W}^T D^\alpha \tilde{W} \\
 &= S_{\text{sum}} \left[ D^{2\alpha-1} (W^T - \hat{W}^T) \varphi - \rho \text{sat} \left( \frac{S_{\text{sum}}}{\theta} \right) \right] \\
 &\quad - \gamma D^{2\alpha-1} \tilde{W}^T D^\alpha \hat{W}.
 \end{aligned}
 \tag{27}$$

The weight adaptive law of RBF neural network is designed as

$$D^\alpha \hat{W} = \frac{1}{\gamma} (S_g + S_c) \varphi.
 \tag{28}$$

Combining Eq. (27) and Eq. (28), it can be obtained

$$\begin{aligned}
 D^\alpha V_2 &\leq S_{\text{sum}} \left[ D^{2\alpha-1} \tilde{W} \varphi - \rho \text{sat} \left( \frac{S_{\text{sum}}}{\theta} \right) \right] \\
 &\quad + \gamma D^{2\alpha-1} \tilde{W}^T D^\alpha \tilde{W} \\
 &= -\rho S_{\text{sum}} \text{sat} \left( \frac{S_{\text{sum}}}{\theta} \right) \leq 0.
 \end{aligned}
 \tag{29}$$

Equation (29) satisfies the Lyapunov stability theory, which indicates the closed-loop system is asymptotically stable. Starting from any initial state, the system can reach the boundary layer in a finite time, and slide along the intersection of two sliding surfaces to the field of zero.

The PMSM fractional order complementary non-singular terminal sliding mode control block diagram based on RBF neural network is shown in Fig. 2.

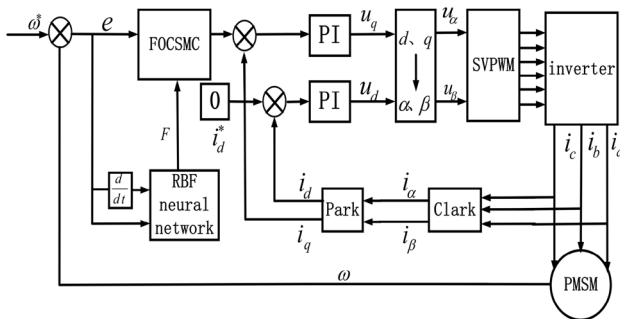


Fig. 2 Block diagram of RBF-FOCSMC

### 4 Simulation Experiment and Analysis

The control system is built in MATLAB/Simulink to verify the effectiveness of the control strategy. Four different control methods are simulated and compared in MATLAB/Simulink environment. Scheme 1 is based on fractional order complementary sliding mode control (FOCSMC); scheme 2 is based on neural network fractional order sliding mode control (RBF-FOSMC); scheme 3 is based on neural network complementary sliding mode control (RBF-CSMC); the fourth scheme is fractional order complementary sliding mode control based on neural network (RBF-FOCSMC). To ensure the fairness, the  $K_p$  and  $K_i$  parameters of the current loop are the same during experiment. The motor parameters are shown in Table 1.

#### 4.1 System Analysis of the Speed Change Response

To study the influence of the motor speed step response, the simulation time is set to 1s and the initial speed step of the motor is set from 0 to 1000 r/min, and then, it is suddenly increased to 1500 r/min at 0.4s, and reduced to 1000 r/min at 0.8s. The speed comparison curves under the four schemes are shown in Figs. 3 and 4.

To explain the dynamic response performance of the system more precisely, the system state time and overshoot of the four schemes are listed in Tables 2, 3, and 4, respectively. As for the system steady-state performance, selecting parts of steady-state speed error curves to zoom in, it is shown in Fig. 5.

From Fig. 4 and Table 2, it can be seen that at the time of the motor start-up, the response time of FOCSMC, RBF-FOSMC, and RBF-CSMC is 0.0160 s, 0.0324 s, and 0.0182 s, respectively, and the speed overshoot is 0.5r/min, 50r/min, and 12r/min, respectively. The response time of RBF-FOCSMC at start-up is 0.0155 s, and there is no speed overshoot. From Fig. 4 and Table 3, it can be seen that when the motor speed increases suddenly from 1000r/min to 1500r/min at 0.4 s, the setting time of FOCSMC, RBF-FOSMC, and RBF-CSMC is 0.0134 s, 0.0240 s, and

Table 1 Motor related parameters

Parameter	Value
Rated power	1.5 [kw]
Pole-pairs	4
Stator inductance	8.5 [mH]
Rotor flux	0.175 [wb]
Stator resistance	2.875 [Ω]
Moment of inertia	0.003 [kg · m <sup>2</sup> ]
Friction coefficient	0.008 [N•m]

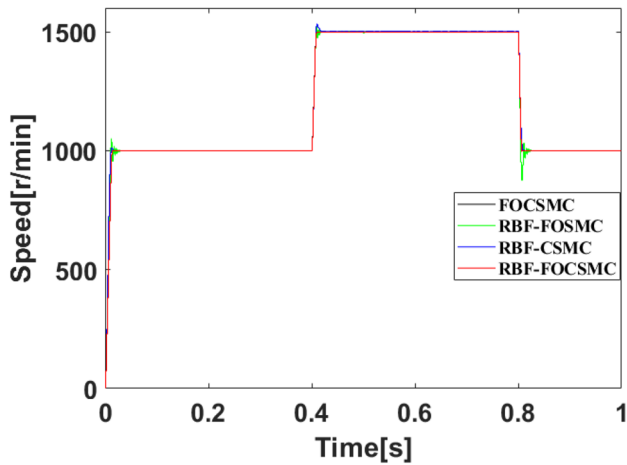


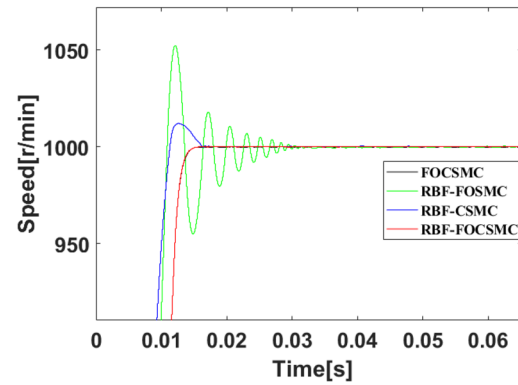
**Fig. 3** Speed comparison curves of four schemes. **a** Speed step local amplification at start-up time. **b** Speed step local amplification at 0.4 s. **c** Speed sudden reduction local amplification at 0.8 s

0.0320 s respectively, and the speed overshoot is 2r/min, 20.1r/min, and 32.8r/min respectively, while the setting time of RBF-FOCSMC is 0.0119 s, and there is also no speed overshoot. From Fig. 4 and Table 4, it can be seen that when the motor speed drops suddenly at 0.8 s, the setting time of FOCSMC, RBF-FOSMC, and RBF-CSMC is 0.0070 s, 0.0250 s, and 0.0130 s, respectively, and the speed overshoot is 3.6r/min, 107r/min, and 2r/min, respectively. The setting time of RBF-FOCSMC is 0.0055 s at start-up, and there is also no speed overshoot. By comparison, RBF-FOCSMC has the fastest response time when the speed increases or decreases, besides, it is stable without overshoot.

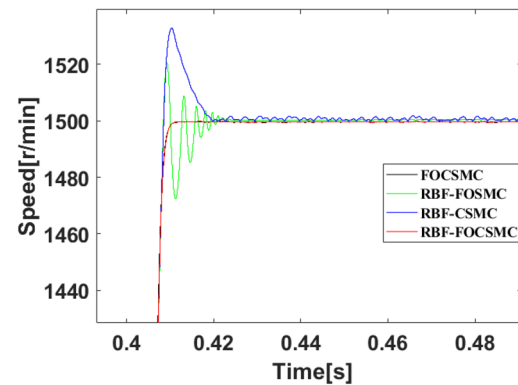
Figure 5 is shown that when the motor entered steady state, the system speed tracking error range of the FOCSMC method is 0.05–0.25r/min, which is about 0.02% of the given speed, and the error range of the RBF-FOCSMC method is 0.08–0.57r/min, which is about 0.065% of the given speed. The system speed tracking error range of RBF-CSMC method is 0.05–0.3r/min, which is about 0.035% of the given speed. The error range of RBF-FOCSMC method is 0.02r/min~0.21r/min, which is about 0.019% of the given speed, it is significantly reduced compared with the former three methods. By comparing the speed tracking error curve, it can be seen that the RBF-FOCSMC method has smaller speed tracking error and smoother control effect.

### 4.2 System Analysis of the Load Change Response

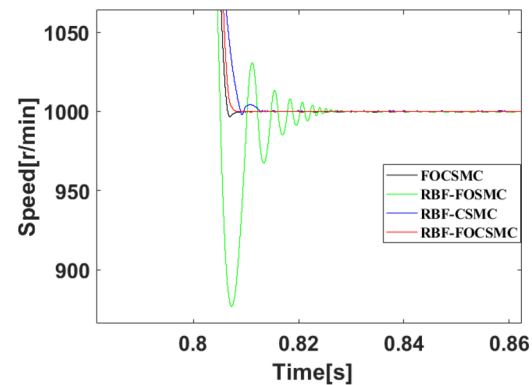
To further verify the anti-load disturbance ability of the proposed method, experiments are carried out for three speed situation: 500r/min, 1000r/min, and 1500r/min. The whole simulation time is 1 s, and the load with 5 N · m and 10 N · m is suddenly added at 0.5s for above three situation. The



(a) Speed step local amplification at start-up time.



(b) Speed step local amplification at 0.4s



(c) Speed sudden reduction local amplification at 0.8s.

**Fig. 4** Speed mutation local amplification curves of four schemes

**Table 2** Performance analysis of four schemes when speed mutation occurs (0–1000r/min)

Scheme category	Setting time [s]	Overshoot [r/min]
FOCSMC	0.0160	0.5
RBF-FOSMC	0.0324	50
RBF-CSMC	0.0182	12
RBF-FOCSMC	0.0155	0

**Table 3** Performance analysis of four schemes when speed mutation occurs (1000–1500r/min)

Scheme category	Setting time [s]	Overshoot [r/min]
FOCSMC	0.0134	2
RBF-FOSMC	0.0240	20.1
RBF-CSMC	0.0320	32.8
RBF-FOCSMC	0.0119	0

**Table 4** Performance analysis of four schemes when speed mutation occurs (1500–1000r/min)

Scheme category	Setting time [s]	Overshoot [r/min]
FOCSMC	0.0070	3.6
RBF-FOSMC	0.0250	107
RBF-CSMC	0.0130	2
RBF-FOCSMC	0.0055	0

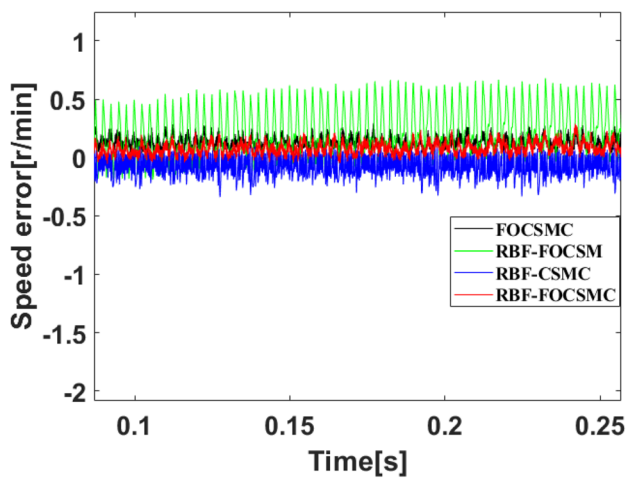
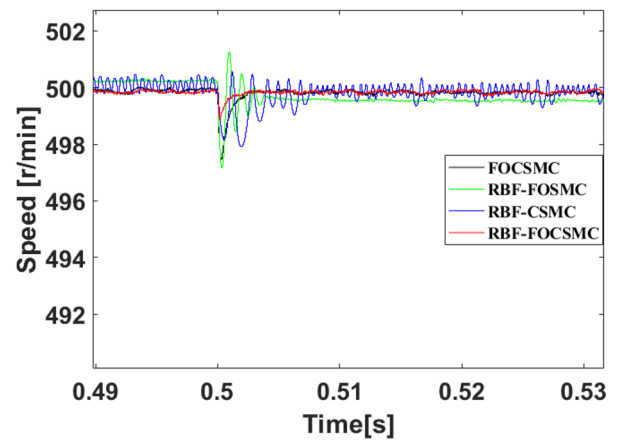


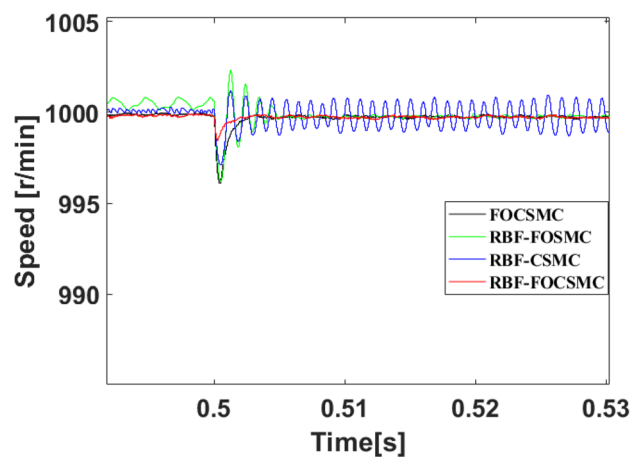
**Fig. 5** Steady-state speed error curves of four schemes

speed response curves under different conditions are shown in Figs. 6 and 7 (Tables 5, 6, 7, 8).

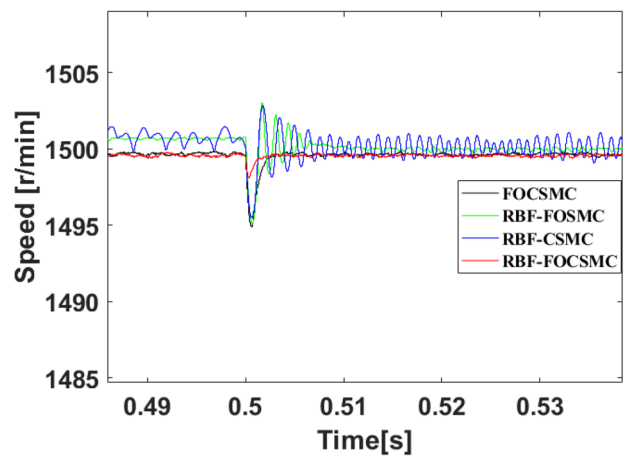
Taking the speed of 1000r/min with  $10 N \cdot m$  load torque disturbance at 0.5 s as an example, from Fig. 7b and Table 9, it can be seen that when the motor is suddenly added load disturbance, the speed of FOCSMC, RBF-FOSMC, and RBF-CSMC decreases by 13.9r/min, 7.8r/min, and 7.2r/min, respectively, and the time to restore stability are 0.0075s, 0.009s, and 0.011s, respectively. The proposed RBF-FOCSMC speed decreases by 3.8r/min, and the time to restore stability after loading is 0.0045s. The detailed experimental results at other speed and load conditions are shown in Tables 5, 6, 7, 8, 9, 10. According to the comparison, in terms of anti-load disturbance ability, the FOCSMC cannot



(a) The speed is 500r/min

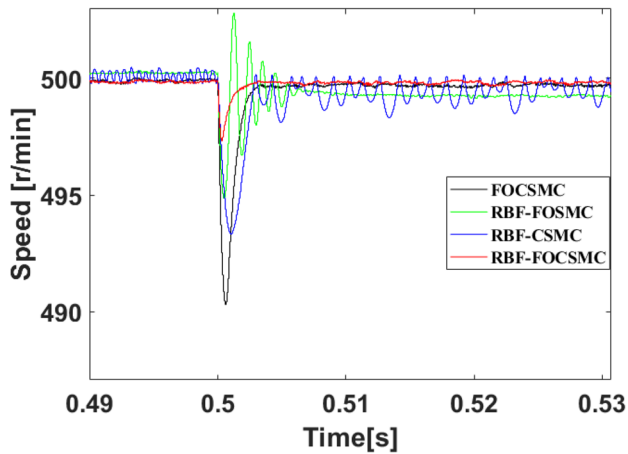


(b) The speed is 1000r/min

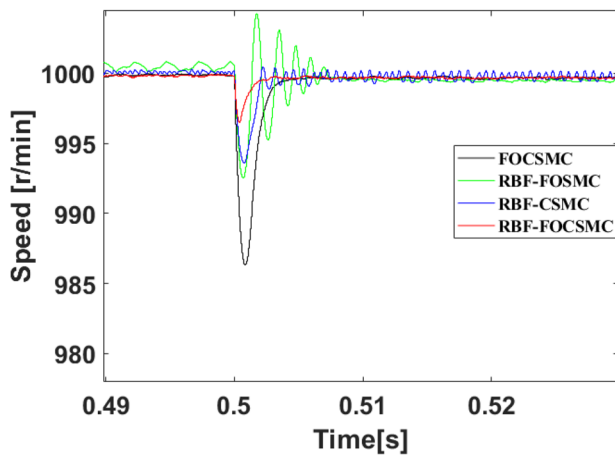


(c) The speed is 1500r/min

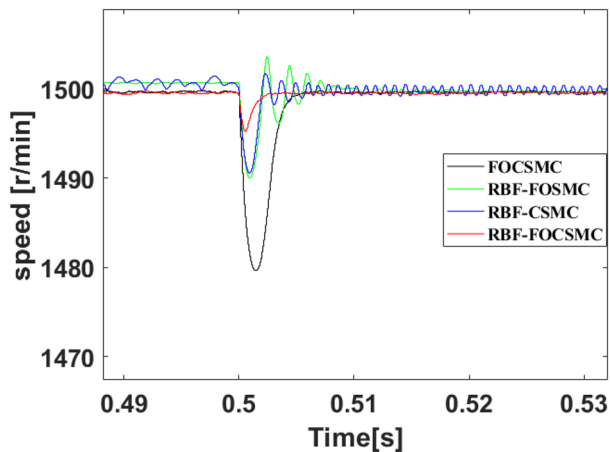
**Fig. 6** Comparison curves of four control methods under load torque disturbance of  $5 N \cdot m$  at 0.5 s. **a** The speed is 500r/min. **b** The speed is 1000r/min. **c** The speed is 1500r/min



(a) The speed is 500r/min



(b) The speed is 1000r/min



(c) The speed is 1500r/min

**Fig. 7** Comparison curves of four control methods under load torque disturbance of  $10 N \cdot m$  at 0.5 s. **a** The speed is 500r/min. **b** The speed is 1000r/min. **c** The speed is 1500r/min

**Table 5** Analysis of four control methods  $5 N \cdot m$  load torque disturbance at 0.5 s (500r/min)

Scheme category	Speed change [r/min]	Setting time [s]
FOCSMC	-2.5	0.004
RBF-FOSMC	-2.8	0.010
RBF-CSMC	-1.9	0.012
RBF-FOCSMC	-1.2	0.003

**Table 6** Analysis of four control methods under  $5 N \cdot m$  load torque disturbance at 0.5 s (1000r/min)

Scheme category	Speed change [r/min]	Setting time [s]
FOCSMC	-3.9	0.005
RBF-FOSMC	-3.8	0.007
RBF-CSMC	-2.8	0.030
RBF-FOCSMC	-1.4	0.004

**Table 7** Analysis of four control methods under  $5 N \cdot m$  load torque disturbance at 0.5 s (1500r/min)

Scheme category	Speed change [r/min]	Setting time [s]
FOCSMC	-5.1	0.008
RBF-FOSMC	-4.8	0.015
RBF-CSMC	-4.5	0.013
RBF-FOCSMC	-2	0.004

**Table 8** Analysis of four control methods under  $10 N \cdot m$  load torque disturbance at 0.5 s (500r/min)

Scheme category	Speed change [r/min]	Setting time [s]
FOCSMC	-10	0.007
RBF-FOSMC	-5.2	0.008
RBF-CSMC	-5.8	0.010
RBF-FOCSMC	-2.8	0.0038

**Table 9** Analysis of four control methods under  $10 N \cdot m$  load torque disturbance at 0.5 s (1000r/min)

Scheme category	Speed change [r/min]	Setting time [s]
FOCSMC	-13.9	0.0075
RBF-FOSMC	-7.8	0.0090
RBF-CSMC	-7.2	0.011
RBF-FOCSMC	-3.8	0.0045



**Table 10** Analysis of four control methods under 10 N·m load torque disturbance at 0.5 s (1500r/min)

Scheme category	Speed change [r/min]	Setting time [s]
FOCSMC	-19.7	0.008
RBF-FOSMC	-9.2	0.014
RBF-CSMC	-8.9	0.015
RBF-FOCSMC	-4.7	0.0050

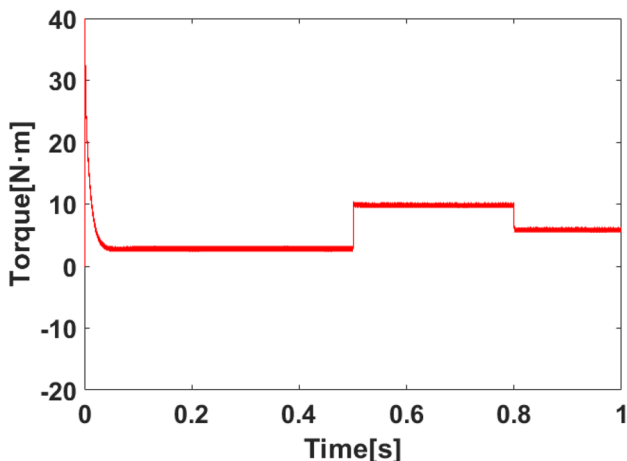


Fig. 8 Motor torque curve

effectively attenuate mismatch disturbance. While the RBF-FOCSMC realizes strong anti-disturbance ability by compensation, it proves that the proposed composite control method has smaller speed fluctuation and faster response.

To verify the tracking performance, the motor is started with a load of 3 N·m, and the load is suddenly increased to 10 N·m at 0.5s and then reduced to 6 N·m at 0.8s. The motor torque response curve is shown in Fig. 8. It can be seen that when the system is affected by the external disturbance, the proposed RBF neural network method can quickly and stably track the system load, and the disturbance estimator is fed back to the speed controller to enhance the anti-interference ability. The three-phase current curves are shown in Fig. 9, which is consistent and proportional to the motor torque.

### 4.3 System Analysis of the Parameter Change Response

To verify the robustness of proposed method with parameter changes, the values of rotor flux and inductance are changed in the experiment, and then, the performances are compared and analyzed. Specifically, the inductance and flux are increased or decreased by 30%, respectively, and the speed is setting to +1000r/min for experiment comparison. The

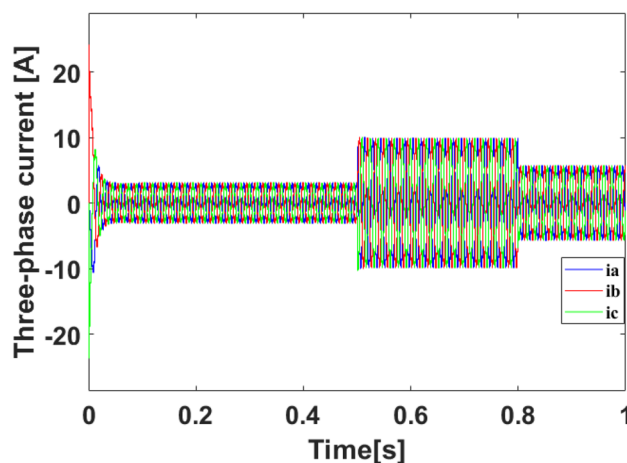
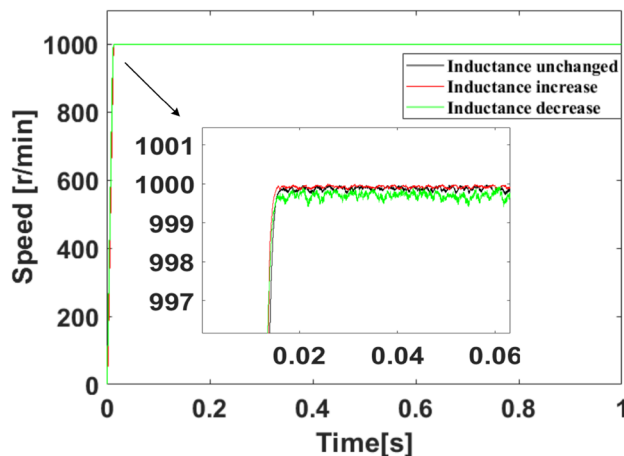
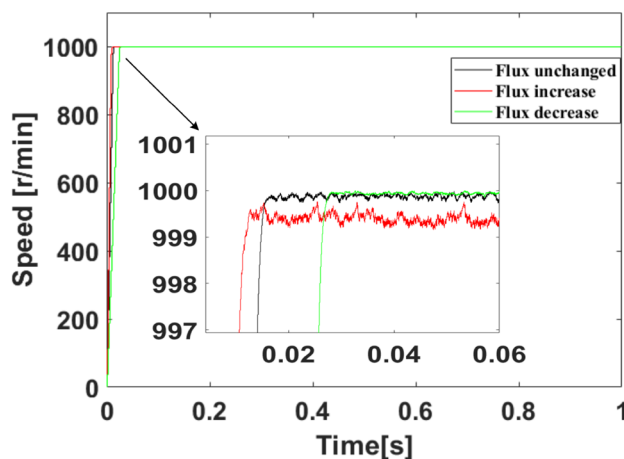


Fig. 9 Three-phase current curve of motor

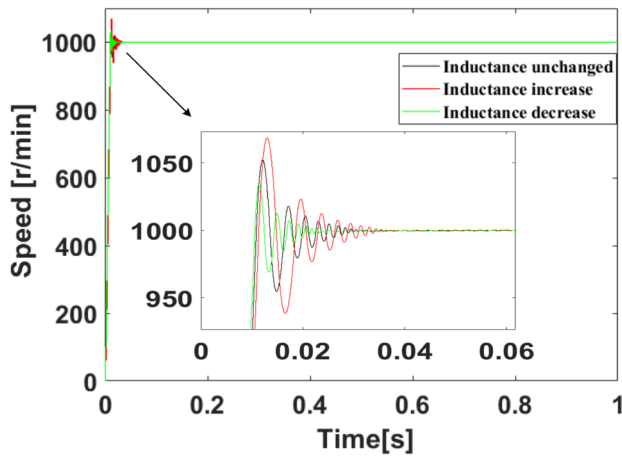


(a) 30% inductance change

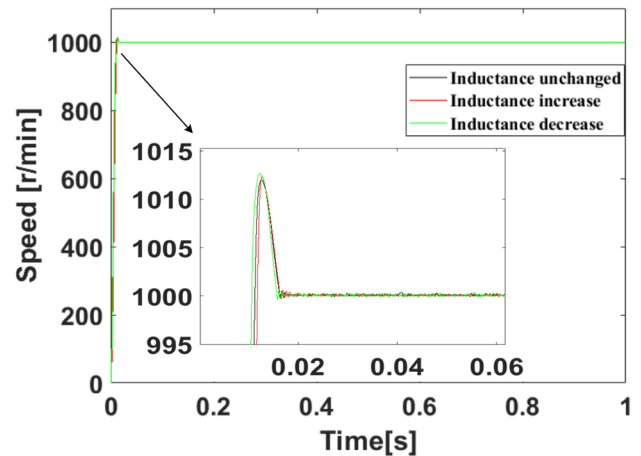


(b) 30% flux change

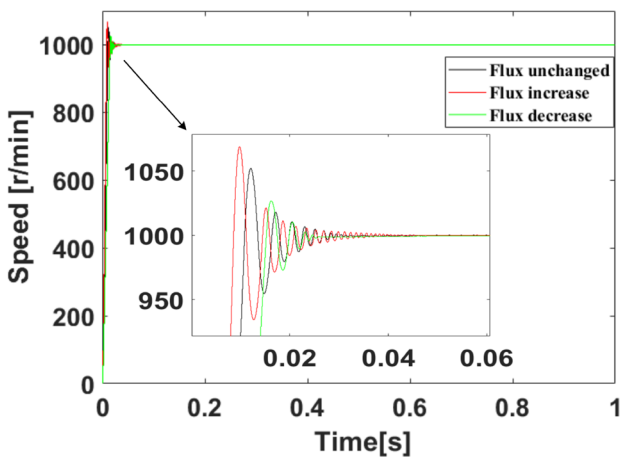
Fig. 10 Comparative curves of FOCSMC method when the parameters are changed by 30%: a 30% inductance change and b 30% flux change



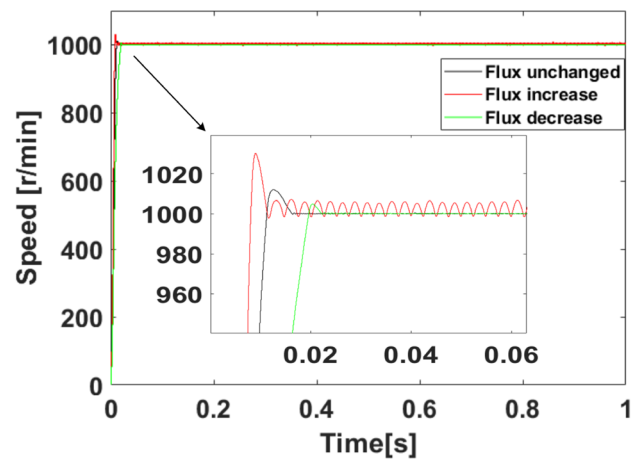
(a) 30% inductance change



(a) 30% inductance change



(b) 30% flux change



(b) 30% flux change

**Fig. 11** Comparative curves of RBF-FOSMC method when the parameters are changed by 30%: **a** 30% inductance change and **b** 30% flux change

results under the four schemes are shown in Figs. 10, 11, 12, 13, and the data analysis are shown in Tables 11, 12, 13, 14.

From Fig. 10 and Table 11, it can be seen that when the motor is rotating with inductance increases or decreases, the speed of FOCSMC method changes by 0.7r/min and 1.1r/min compared with the normal condition, and the response time changes by 0.0005s; when the flux linkage increases and decreases, the speed changes by 0.9r/min and 0.6r/min compared with the normal conditions, and the response time changes by 0.0007s and 0.011s.

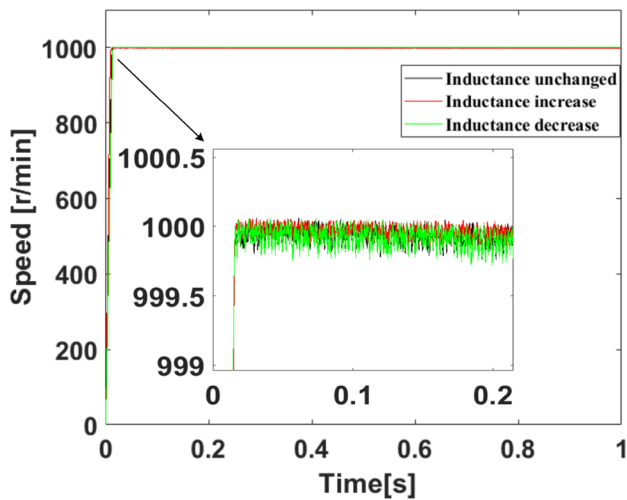
From Fig. 11 and Table 12, it can be seen that when the motor is rotating with inductance increases or decreases, the speed of the RBF-FOCSMC method changes by 15r/min and 15.5r/min compared with the normal condition, and the response time changes by 0.0026s and 0.0074s, respectively. When the flux linkage increases and decreases, the speed

**Fig. 12** Comparative curves of RBF-CSMC method when the parameters are changed by 30%: **a** 30% inductance change and **c** 30% flux change

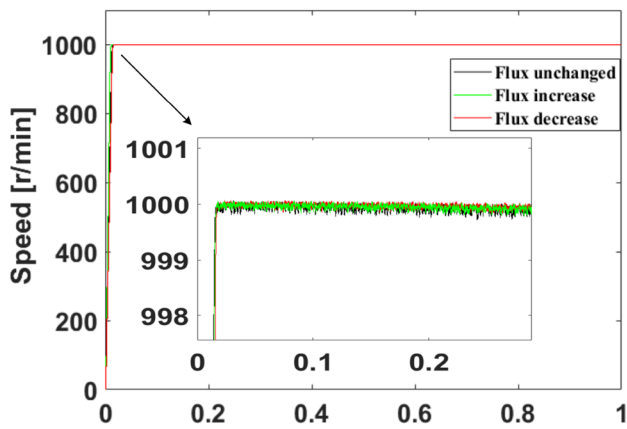
changes by 18.5r/min and 15r/min compared with normal condition, and the response time changes by 0.0056s and 0.0064s.

From Fig. 12 and Table 13, it can be seen that when the motor is rotating with inductance increases or decreases, the speed of the RBF-CSMC method changes by 0.4r/min and 0.8r/min compared with the normal condition, and the response time changes by 0.0018s and 0.0028s, respectively. When the flux linkage increases and decreases, the speed changes by 18.1r/min and 7.1r/min compared with the normal conditions, and the response time changes by 0.0042s and 0.0043s.

From Fig. 13 and Table 14, it can be seen that when the motor is rotating with inductance increases or decreases, the speed of the RBF-FOCSMC method changes by 0.1r/min



(a) 30% inductance change



(b) 30% flux change

**Fig. 13** Comparative curves of RBF-FOCSMC method when the parameters are changed by 30%: **a** 30% inductance change and **b** 30% flux change

**Table 11** Performance analysis of FOCSMC control method under parameter change

Parameter change	Speed change [r/min]	Recovery time [s]
Inductance increase	-0.2	0.0005
Inductance decrease	-0.6	0.0005
Flux induction	-0.4	0.0007
Flux decrease	-0.1	0.011

and 0.2r/min compared with the normal condition, and the response time changes by 0.0006s and 0.0003s, respectively. When the flux linkage increases and decreases, the speed changes by 0.1r/min and 0.1r/min compared with the normal

**Table 12** Performance analysis of RBF-FOSMC control method under parameter change

Parameter change	Speed change [r/min]	Recovery time [s]
Inductance increase	+ 65	0.0026
Inductance decrease	+ 34.5	0.0074
Flux induction	+ 68.5	0.0056
Flux decrease	+ 35	0.0064

**Table 13** Performance analysis of RBF-CSMC control method under parameter change

Parameter change	Speed change [r/min]	Recovery time [s]
Inductance increase	+ 12.4	0.0018
Inductance decrease	+ 12.8	0.0028
Flux induction	+ 30.1	0.0042
Flux decrease	+ 4.9	0.0043

**Table 14** Performance analysis of RBF-FOCSMC control method under parameter change

Parameter change	Speed change [r/min]	Recovery time [s]
Inductance increase	-0.1	0.0006
Inductance decrease	-0.2	0.0003
Flux induction	-0.1	0.0003
Flux decrease	-0.1	0.0001

conditions, and the response time changes by 0.0003s and 0.0001s.

From the results of four comparative experiments, it can be seen that RBF-FOCSMC has little impact on speed tracking and response time compared with normal condition. Therefore, the designed RBF-FOCSMC has good anti-parameter disturbance ability.

### 5 Conclusion

In this paper, a control strategy combining RBF neural network and complementary fractional non-singular terminal sliding mode control is designed. The fractional order complementary non-singular terminal sliding mode is used to improve the static and dynamic tracking performance of the motor. While improving the tracking accuracy, the steady-state error is reduced, and finally, the effect of suppressing chattering is achieved. The RBF neural network is used to approximate the disturbance and

un-modeled parts of the system, which perform feedback compensation to further improve the dynamic response ability and anti-interference ability of the system. The experimental results prove the feasibility of the proposed algorithm, which shows obvious control effect; it has higher tracking accuracy and faster response than the ordinary sliding mode control method. Therefore, the proposed method can provide an ideal method for motor control system, and also give a theoretical support for improving the PMSM control accuracy of electric vehicles. While due to the limitations of the current experimental conditions and environment, only the simulation experiment is verified in this paper, the physical experiment will be studied and focused on the future work.

**Acknowledgements** This work is supported by Scientific Research Program of Hubei Provincial Department of Education (D20221802), Reveal List Technology Project of Hubei Province (2021BEC002), and Scientific Research Program of Hubei Provincial Department of Education (Q20221805).

## References

- Bai, C., Yin, Z. Y., Zhang, Y. Q., & Liu, J. (2022). Robust predictive control for linear permanent magnet synchronous motor drives based on an augmented internal model disturbance observer. *IEEE Transactions on Industrial Electronics*, *69*(10), 9771–9782.
- Cai, B. P., Zhao, Y. B., Liu, H. L., & Xie, M. (2017). A data-driven fault diagnosis methodology in three-phase inverters for PMSM drive systems. *IEEE Transactions on Power Electronics*, *32*(7), 5590–5600.
- Cao, H. Y., Deng, Y. T., Li, H. W., Wang, J. L., Liu, X. F., Sun, Z., & Yang, T. (2023). Generalized active disturbance rejection with reduced-order vector resonant control for PMSM current disturbances suppression. *IEEE Transactions on Power Electronics*, *38*(5), 6407–6421.
- Du, H. M., Gao, H., Hu, Z. H., Shen, Y. P., & Fan, M. J. (2022). Design of the active disturbance rejection speed regulation system of super-twisting sliding mode for permanent magnet synchronous motors. *Journal of Chongqing University of Technology (natural Science)*, *36*(10), 216–222.
- Duarte-Mermoud, M. A., Aguila-Camacho, N., Gallegos, J. A., & Castro-Linares, R. (2015). Using general quadratic Lyapunov functions to prove Lyapunov uniform stability for fractional order systems. *Communications in Nonlinear Science and Numerical Simulation*, *22*(1–3), 650–659.
- Jin, P. (2021). Research and application on PMSM servo system based on fuzzy fractional order sliding mode algorithm. *Machinery Design & Manufacture*, *366*(08), 270–274.
- Jin, H. Y., & Zhao, X. M. (2019). Complementary sliding mode control via elman neural network for permanent magnet linear servo system. *IEEE Access*, *7*, 82183–82193.
- Jin, H. Y., & Zhao, X. M. (2020). Speed control of permanent magnet linear synchronous motor based on complementary sliding mode control and iterative learning control. *Control Theory & Applications*, *37*(04), 918–924.
- Li, T. C., Zhao, Y. J., & Hou, L. M. (2023). Adaptive sliding mode control with disturbance observer for speed regulation system of permanent magnet synchronous motor. *IEEE Access*, *11*, 17021–17030.
- Li, Y. H., Zhao, C. H., Zhou, Y. F., & Qin, Y. G. (2022). Deep neural network control for PMSM based on data drive. *Electric Machines and Control*, *26*(1), 115–125.
- Li, T., Liu, X. D., & Yu, H. S. (2021). Backstepping nonsingular terminal sliding mode control for PMSM with finite-time disturbance observer. *IEEE Access*, *9*, 135496–135507.
- Liu, K. W. (2014a). *Stability of fractional order differential systems*. Hefei: Anhui University.
- Liu, J. K. (2014b). *RBF neural network control for mechanical systems: design analysis and MATLAB simulation*. Bei Jing: tsinghua University Press.
- Lu, C. H., Tai, C. C., Chen, T. C., & Wang, W. C. (2015). Fuzzy neural network speed estimation method for induction motor speed sensorless control. *International Journal of Innovative Computing Information and Control*, *11*(2), 433–446.
- Podlubny, I. (1999). *Fractional differential equations*. London: Academic Press.
- Wang, G. (2020). Eso-based terminal sliding mode control for uncertain full-car active suspension systems. *Int. J. Automotive Technology*, *21*(3), 691–702.
- Xu, Y., Lin, C., & Xing, J. L. (2023). Transient response characteristics improvement of permanent magnet synchronous motor based on enhanced linear active disturbance rejection sensorless control. *IEEE Transactions on Power Electronics*, *38*(4), 4378–4390.
- Yu, J. P., Dong, W. J., Chen, B., & Lin, C. (2015). Neural network-based adaptive dynamic surface control for permanent magnet synchronous motors. *IEEE Transactions on Neural Networks and Learning Systems*, *26*(3), 640–645.
- Zhang, J. L., Chen, Y. F., Gao, Y., Wang, Z. H., & Peng, G. S. (2021). Cascade ADRC speed control base on FCS-MPC for permanent magnet synchronous motor. *Journal of Circuits, Systems, and Computers*, *30*(11), 22.

**Publisher's Note** Springer Nature remains neutral with regard to jurisdictional claims in published maps and institutional affiliations.

Springer Nature or its licensor (e.g. a society or other partner) holds exclusive rights to this article under a publishing agreement with the author(s) or other rightsholder(s); author self-archiving of the accepted manuscript version of this article is solely governed by the terms of such publishing agreement and applicable law.